ORIGINAL ARTICLE

Abrupt increase in Greenland melt enhanced by atmospheric wave changes

Rune Grand Graversen[1,2] · Tuomas Heiskanen[1] · Richard Bintanja[3] · Heiko Goelzer[4]

© The Author(s) 2024

Abstract

Recent Greenland ice-sheet melt constitutes a considerable contribution to global sea-level rise. Observations indicate an approximate zero mass balance of the ice sheet until the late 1990s, after which a strong increase in melting occurred. This cannot be attributed linearly to gradually-increasing global warming. Instead the abrupt shift has been linked to atmospheric circulation changes, although causality is not fully understood. Here we show that changes of atmospheric waves over Greenland have significantly contributed to the shift into a strong melting state. This is evident after having applied a newly-developed methodology effectively decomposing atmospheric flow patterns into parts associated with waves of different scales such as Rossby waves and smaller perturbations. The onset of a westerly-flow reduction, consistent with anthropogenic Arctic warming, affected transports by atmospheric waves and led to a decrease in precipitation and an increase in surface warming, contributing to ice-sheet mass loss, in particular over the southwestern regions. As such, the Greenland ice-sheet melt is an example of a climate response non-linearly coupled to global warming.

1 Introduction

Sea-level rise is a major threat to humanity. The Greenland ice sheet has since the late 1990s experienced a substantial mass loss (Katsman et al. 2011; Mouginot et al. 2019; Bevis et al. 2019; IMBIETeam 2020; Hanna et al. 2020), which

✉ Rune Grand Graversen
  rune.graversen@uit.no

  Tuomas Heiskanen
  tuhe@dips.no

  Richard Bintanja
  bintaja@gmail.com

  Heiko Goelzer
  heig@norceresearch.no

1 Department of Physics and Technology, University of Tromsø (UiT), Tromsø, Norway

2 Norwegian Meteorological Institute, Tromsø, Norway

3 Royal Netherlands Meteorological Institute (KNMI), De Bilt, The Netherlands

4 NORCE Norwegian Research Centre, Bjerknes Centre for Climate Research, Bergen, Norway

is unprecedented since the beginning of the mid-Holocene (about 8 thousand years ago; Yang et al. 2022). This has severe implications for ongoing and future global sea-level rise, should the melting pace continue (IPCC 2021). In addition, the melting has led to increased release of methane from the ice-sheet bed (Lamarche-Gagnon et al. 2019), contributing to further greenhouse-gas-induced global warming.

The ice-sheet mass loss is the largest along the margins of the ice sheet—in particular in the southwestern part of Greenland (Mouginot et al. 2019; Bevis et al. 2019; IMBIETeam 2020)—and is mainly a consequence of increased losses associated with the surface mass balance (SMB, accumulation minus ablation; Mouginot et al. 2019; van Kampenhout et al. 2020), although increase of discharge of marine-terminating outlet glaciers (dynamical discharge) also provides a significant contribution (IMBIETeam 2020; King et al. 2020; Choi et al. 2021). If increased runoff due to melting is not balanced by an opposing increase in precipitation or reduction in discharge, the ice sheet loses mass.

It has been argued that atmospheric processes play an important role in this strong recent mass loss (Hanna et al. 2013; Fettweis et al. 2013; Ding et al. 2014; van den Broeke et al. 2017; Hofer et al. 2017; Hanna et al. 2018; Bevis et al.

2019; Oltmanns et al. 2019; Hanna et al. 2020; Izeboud et al. 2020; Hanna et al. 2021; Matsumura et al. 2021; Wachowicz et al. 2021). Surface melt occurs when energy convergence of various energy fluxes raises the temperature to the melting point, which predominantly occurs close to the atmosphere-ice interface, and is therefore associated with the surface energy balance.

The surface energy balance includes net solar radiation (downward minus reflected), net longwave radiation (downward minus emitted) and net turbulent heat and moisture fluxes where the latter is a latent heat flux associated with sublimation and icing—deposition of frost and frozen dew. A positive surface energy balance provides energy to heat the surface when frozen, and for melting when local temperatures are above the freezing point.

Turbulent heat fluxes of both the sensible and latent type can be important drivers of extreme melt events of the Greenland ice sheet (Mattingly et al. 2020). For example the turbulent heat fluxes were as important as the radiative effects (Fausto et al. 2016), during the severe melt in summer of 2012 (Hanna et al. 2014).

Clouds, humidity, and temperature over the ice sheet strongly control downwelling short and longwave radiation as well as the turbulent fluxes at the atmosphere–ice interface, and are hence important for the ice melt. For instance clouds have mostly a net heating effect over the ice sheet (Mattingly et al. 2018; Izeboud et al. 2020; Mattingly et al. 2020), although clouds can cause cooling in case the albedo of the ice-sheet surface is low (Hofer et al. 2017). In addition, atmospheric processes may affect dynamical discharge, as melt water induced by atmospheric forcing can penetrate to the bottom of the ice sheet where it causes increased lubrication hereby affecting the speed of outlet glaciers. Plumes of subglacial discharge may also enhance melting at the calving front (Slater and Straneo 2022). And changes of atmospheric processes may lead to increase of temperatures of the fjord waters which can enhance melting of floating outlet glaciers (Inall et al. 2014; Wood et al. 2021). However, these impacts are complex and it is unclear whether the net effect is a speed-up or a slow-down of the outlet streams (Sundal et al. 2011).

Many of these processes are considerably controlled by the atmospheric circulation. Several studies have suggested that modes of variability such as the North-Atlantic Oscillation (NAO) and the Greenland Blocking Index (GBI) have changed, hereby inducing Greenland ice-sheet melt (Mote 1998; Hanna et al. 2013; Hofer et al. 2017; Bevis et al. 2019; Hanna et al. 2020; Henderson et al. 2021), although blocking indices are prone to some uncertainties (Wachowicz et al. 2021). The GBI has been increasing in all seasons since beginning of the 1980s with particular strong increase in the summer season (Hanna et al. 2016; Wachowicz et al. 2021), which is however not supported by models (Hanna et al.

2018). Also it has been argued that Rossby-wave trains of tropical origin (Ding et al. 2014) and El-Ninõ-induced intensification of extratropical cyclones (Matsumura et al. 2021) have an impact on Greenland temperatures and hence on the ice-sheet SMB. At the Greenland latitudes, most circulation patterns occur in the form of atmospheric waves, such as Rossby waves and cyclones. These bring heat and moisture over the ice sheet. This raises the question: how is the Greenland ice-sheet melt linked to these atmospheric waves? By estimating SMB changes related to heat and moisture transport by atmospheric waves, we here provide a more direct and quantitative estimate of the impact of atmospheric circulation on the Greenland SMB than was previously given based on circulation indices. The atmospheric waves and their transport of heat and moisture impact the SMB through alteration of both the surface energy balance and precipitation. After having presented the data and methods, we discuss these couplings.

2 Data and methods

We use atmospheric fields from the ERA5 reanalysis, and Greenland ice-sheet surface mass balance from the Regional Atmospheric Climate Model (RACMO2) based on downscaling of the ERA Interim reanalysis. All data are for the period 1979–2018.

2.1 Atmospheric data and wave decomposition

The atmospheric data are taken from the ERA5 reanalysis (Hersbach et al. 2020). The ERA5 reanalysis has a global coverage, a T639 horizontal resolution corresponding to about 0.25° × 0.25°, and 137 hybrid (sigma/pressure) levels. The ERA5 reanalysis is shown to perform among the best reanalysis for the Arctic area (Graham et al. 2019). The atmospheric energy transport may be decomposed into dry-static (plus kinetic), $D = c_p T + gz + \mathbf{v}^2/2$, and latent, $Q = Lq$, transport components (Oort and Peixóto 1983), where c_p is the specific heat capacity at constant pressure, T temperature, g gravitational acceleration, z geopotential heights, L latent heat of condensation, q specific humidity, and $(u, v) = \mathbf{v}$ the zonal and meridional velocity components. The dry-static part includes enthalpy (sensible heat), potential energy and—due to tradition—kinetic energy (which however is small compared to the other energy contributions). The latent part is associated with the transport of moisture. Reanalysis data such as those of ERA5 are subjected to a mass-flux inconsistency (Trenberth 1991); therefore a mass-flux correction is applied to the wind field at each time step, before computing the energy transport (Graversen 2006). The atmospheric heat transport may be further divided into waves through a

Fourier decomposition in the zonal direction (Baggett and Lee 2015; Graversen and Burtu 2016; Heiskanen et al. 2020). Based on wave numbers in the mass-flux field, the transport is hereby split into synoptic-scale and planetary-scale contributions (Rydsaa et al. 2021). Planetary waves are typically Rossby waves, while synoptic systems include cyclones and mesoscale and other small-scale disturbances. For the dry-static component, the meridional transport decomposition into the two length scales, Rossby waves and synoptic-scale waves, yields:

$$vD_p(\phi, \lambda, t) = \sum_{\eta=1}^{H} \left(\frac{a_0}{2} + \sum_{n=1}^{3} (a_n \cos(n\lambda) + b_n \sin(n\lambda)) \right) D \tag{1}$$

and

$$vD_s(\phi, \lambda, t) = \sum_{\eta=1}^{H} \left(\sum_{n \geq 4} (a_n \cos(n\lambda) + b_n \sin(n\lambda)) \right) D, \tag{2}$$

respectively, where, ϕ and λ are latitude and longitude coordinates (in radians), t time, η hybrid level, and H is the number of hybrid levels. The dry-static energy, $D(\phi, \lambda, \eta, t)$, is a function of three-dimensional space and time, and $a_n(\phi, \eta, t)$ and $b_n(\phi, \eta, t)$ are the Fourier coefficients, as a function of latitude, height, and time, of the meridional mass flux $v \times dp/g$, where $dp(\phi, \lambda, t)$ is the pressure difference between two hybrid half levels, $\eta - 1/2$ and $\eta + 1/2$, and a function of horizontal space and time. Similarly, the zonal energy transport, $uD(\phi, \lambda, \eta, t)$, is decomposed using a Fourier decomposition in the zonal direction of the zonal mass flux, $u \times dp/g$. The latent energy transport is decomposed in a similar way. The energy transport components are calculated from ERA5 instantaneous fields of T, q, u, and v on model hybrid levels, and p_s and Z0, where the former is surface pressure and the latter the topography. All fields are at a $0.25° \times 0.25°$ horizontal resolution, and a six-hour time resolution (except Z0 which is constant in time).

Based on previous studies (Heiskanen et al. 2020; Rydsaa et al. 2021), the separation between large and small-scale waves is set between wavenumbers $n = 3$ and $n = 4$, as indicated in Eqs. 1 and 2. The zonal-mean flow component given by the wavenumber $n = 0$ is included in the large-scale wave components $n = 1-3$ (Eq. 1). In previous studies (Graversen and Burtu 2016; Heiskanen et al. 2020), where only the meridional component of the energy transport is considered, the contribution of $n = 0$ is small at high latitudes. However, when the zonal energy-transport component is taken into account, as is done here, the zonal-mean part is considerable. As the zonal-mean part is a large-scale component it is here considered along with the large-scale waves. The convergences of dry-static and latent energy transport by Rossby waves yields:

$$D_p^{conv}(\phi, \lambda, t) = -\nabla_z \cdot (uD_p, vD_p) \tag{3}$$

and

$$Q_p^{conv}(\phi, \lambda, t) = -\nabla_z \cdot (uQ_p, vQ_p,), \tag{4}$$

respectively, where D_p^{conv} is the dry-static and Q_p^{conv} the latent transport convergence of Rossby waves, and ∇_z is the horizontal divergence operator. In a similar way, convergence of dry-static and latent energy convergence by the synoptic waves, D_s^{conv} and Q_s^{conv} can be estimated from (uD_s, vD_s) and (uQ_s, vQ_s), respectively. To reduce spatial noise, the convergence fields are spatially smoothed by employing a weighted running average over two degrees in the latitude direction and over an equal distance in the longitude direction.

2.2 Surface mass balance and surface energy balance

The SMB is provided by the polar version of the Regional Atmospheric Climate Model (RACMO2) (Noël et al. 2018). The RACMO2 regional model is run on a 5.5 km horizontal grid-resolution over the Greenland area, and the output is statistically down-scaled to a 1 km grid in order to compute the SMB. The RACMO2 model is forced with ERA-Interim on the boundaries, and the SMB is computed using a multi-layer snow module (Ettema et al. 2010). The RACMO2-down-scaled SMB is found to be among the most accurate compared to other model results (Fettweis et al. 2020). The SMB is defined as:

$$SMB = PR - SU - EW - RU, \tag{5}$$

where PR is precipitation, SU sublimation, EW wind erosion, and RU runoff. Liquid water mass from melt or rainfall may percolate through the firn layer, and be retained, either through refreezing or capillary forces. The remaining part of the liquid water runs off. The runoff, RU, consists of the melt water, ME, and rainfall, RA, from which the irreducible water, RZ, and refrozen water, CR, are subtracted:

$$RU = ME + RA - RZ - CR. \tag{6}$$

The melt water is dependent on the energy balance of the surface layer (SEB):

$$SEB = SW_{net} + LW_{net} + SHF + LHF + G_s + R, \tag{7}$$

where SW_{net} is the net shortwave radiation at the surface, LW_{net} the net longwave radiation, SHF the sensible heat flux, LHF the latent heat flux, G_s the subsurface heat flux, and R is associated with cooling rain water which can provide a small energy input to the ice sheet, in particular at the southern margins where rain is frequently occurring (Doyle et al. 2015; Fausto et al. 2016; Niwano et al. 2021). The SEB and

precipitation is obtained from ERA5. The SEB is computed as in Eq. 7, but without the subsurface heat fluxes and cooling rain, as these are small.

2.3 Regressions

Linear regressions of the SMB on components of the energy-transport convergence, surface energy balance, and precipitation are performed with daily data on a $0.25° \times 0.25°$ grid, which is about the resolution of the ERA5 data. Hence the SMB data from the high-resolution RACMO2 model are first interpolated to the ERA5 grid. Anomalies of these fields are obtained by subtracting a five-year running climatology with daily resolution whereby both the annual cycle and trends are suppressed, following a procedure described and applied in Kapsch et al. (2019). The climatology is smoothed with a 10-day running-mean filter prior to the subtraction, and the anomaly fields are likewise smoothed with a 10-day running-mean filter in order to suppress variability below the synoptic time-scale. The regression coefficients are now computed; for example the regression of the SMB on the dry-static planetary-wave convergence yields:

$$\beta_{D_p}^{\mathrm{SMB}} = \frac{\mathrm{cov}\left[\mathrm{SMB}, D_p^{\mathrm{conv}}\right]}{\mathrm{var}\left[D_p^{\mathrm{conv}}\right]}, \tag{8}$$

where cov[·, ·] and var[·] indicates covariance and variance, respectively.

Statistical significance is tested using a Monte-Carlo approach: Artificial time series with the same power spectrum as the original one are constructed by randomly interchanging phases of the Fourier modes in the time dimension. A two-sided test is conducted by comparing the regressions based on the artificial times series with that of the original for each spatial grid point. The Monte-Carlo significance test is based on at least 2000 artificial time series. This approach avoids assumptions regarding distribution of data.

2.4 Trends

The trends and circulation changes are computed by subtracting the mean state of the period after year 2000 from that before. The separation of periods is chosen at year 2000 due to the acceleration of the mass loss starting approximately in year 2000. The contribution of a given energy-transport component to the SMB trend is obtained by multiplying trends of that component with its regression coefficients. Hereby the part of the SMB trend "explained" by a given energy transport component is derived. For example the part of the SMB trend associated with the dry-static planetary wave convergence yields:

$$\delta \mathrm{SMB}^{D_p}(\phi, \lambda) = \beta_{D_p}^{\mathrm{SMB}} \delta D_p^{\mathrm{conv}}, \tag{9}$$

where $\delta D_p^{\mathrm{conv}}$ is the trend of D_p^{conv}.

The statistical significance of the trends is tested by performing a two-sided Monte-Carlo sampling using at least 2000 iteration by random permutation. To account for the auto-correlation of the time-series, the random sampling is performed by making random permutations of the years.

The time evolution of the SMB associated with an energy-transport-convergence component is calculated as:

$$SMB^{D_p}(\phi, \lambda, t) = \beta_{D_p}^{SMB} D_p^{\mathrm{conv}}, \tag{10}$$

using again the component D_p^{conv} as an example. Here the convergence anomalies are based on subtracting climatology of all years in the data set in contrast to subtracting a 5-year running-mean climatology as applied for the regressions as explained above. The reason for the different approach is that here the trend should be retained in the anomaly data. The SMB and its parts associated with the transport components and the zonal mass flux in the southwest Greenland (Figs. 3b and S6) are computed by time-averaging into monthly data, summing over this region, and finally applying a 36-months running-mean filter on the resulting time series.

3 Results

3.1 Surface energy balance

A negative SMB is associated with melting and hence with net convergence of energy flux in the ice sheet, in particular in the surface-near layer below the atmosphere–ice interface. In this layer, convergence of energy flux is mostly due to the surface energy balance (see Sect. 2.2), since energy flux from below and laterally within the ice is small. Regressions of the SMB on the surface energy balance (see Sect. 2.3) shows that a positive energy balance implies a negative SMB at the western and northern ice-sheet margins, but a positive SMB in the interior and eastern margins (Fig. 1a). The latter pattern is due to a strong correlation between surface energy balance and precipitation that appears since cloudy weather leading to precipitation is also causing positive energy-flux anomalies at the surface. When removing the part of the surface energy balance that is temporally correlated with precipitation before computing the regressions (by applying a decorrelation approach; see Appendix), the regression coefficients show mostly clearly negative or little SMB impact along the margins, and little response in the interior where temperatures are mainly bellow the freezing point, even during positive surface-energy-balance anomalies (Fig. 1b). Hence a positive energy balance causes melting and a negative SMB in areas where the temperature can easily reach the
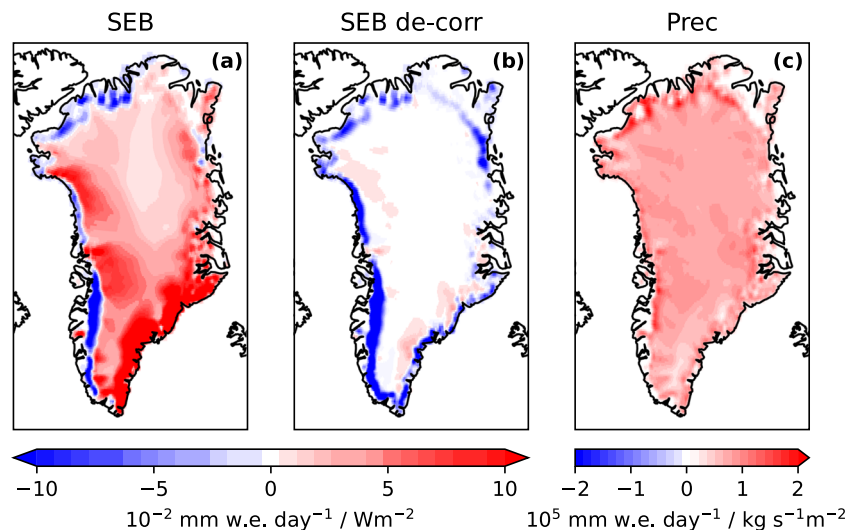
Fig. 1 Impact of the surface energy balance and precipitation on the SMB. Regressions of the SMB on the surface energy balance (**a**), the part of the surface energy balance that is decorrelated with (orthogonal to; see Appendix) precipitation (**b**), and precipitation (**c**). Virtually all shaded areas are significant on the 99% level based on a Monte-Carlo approach randomly interchanging phases (Fig. S1; see Sect. 2.3). The surface energy balance and precipitation are based on the ERA5 reanalysis whereas the SMB is from the RACMO regional model, based on a downscaling of the ERA-Interim reanalysis. The SMB is in units of mm water equivalent per day

melting point. Predominantly negative temperatures are also prevailing at high altitudes in the mountains in the southeast where accordingly the SMB impact of the surface energy balance is less negative as compared the ice-sheet margin in the southwest. Precipitation, although not decorrelated with the surface energy balance, provides a positive SMB over the entire ice sheet, but mainly so at the ice-sheet margins where topography gradients are the largest (Fig. 1c). Hence, the regressions reveal that both the surface energy balance and precipitation play an important role for the SMB, and the impact is opposite for the two variables.

The surface energy balance is controlled by atmospheric conditions such as clouds, humidity and temperature. These quantities are strongly influenced by advection due to the atmospheric circulation. Hence as a consequence of this chain of processes, it can be hypothesised that the atmospheric circulation provides a strong control over the SMB. As mentioned above, several studies have indicated changes in the atmospheric circulation over Greenland during the past decades, and that these changes indeed have had an impact on the SMB (Hanna et al. 2013; Fettweis et al. 2013; Ding et al. 2014; van den Broeke et al. 2017; Hofer et al. 2017; Hanna et al. 2018; Bevis et al. 2019; Olt-manns et al. 2019; Izeboud et al. 2020; Hanna et al. 2020, 2021; Matsumura et al. 2021; Wachowicz et al. 2021). It has been noted that a general increase in moistening of the Arctic atmosphere is associated with changes in north-ward latent heat transport (Nygård et al. 2020). It has also been argued that blocking events over Greenland lead to transport of warm and moist air over the ice sheet (Barrett

et al. 2020; Sherman et al. 2020), affecting both the surface energy balance and precipitation. Strong moisture advection events—known as atmospheric rivers—are associated with increase in clouds, temperature, and winds which lead to a positive surface energy balance especially due to the turbulent sensible heat flux (Mattingly et al. 2020). In addition, temperatures at coastal stations are correlated with indices of atmospheric modes such as the North-Atlantic Oscillation (NAO; Hanna et al. 2014, 2020, 2021).

Atmospheric circulation transports both sensible heat (dry-static energy) and moisture, and the convergence of these transport components over Greenland will affect both surface energy balance and precipitation, hence having often opposite SMB impacts (Fig. 1). Therefore, in order to estimate this linkage between atmospheric circulation and the SMB, it is important to decompose the transport into its components.

3.2 Atmospheric energy advection over Greenland

The energy transport by the atmospheric circulation can be decomposed into a dry-static and a latent component, where the former is associated with the advection of sensible heat and the latter with moisture (see Sect. 2.1). Convergence of these two components leads to an increase of energy transfer to the surface (Graversen and Burtu 2016). The latent component affects the surface energy balance considerably more than its dry-static counterpart (Graversen and Burtu 2016), since convergence of this component leads to an increase in water-vapour and clouds which increase

downward longwave radiation at the surface. In addition, as discussed above, the latent transport convergence induces precipitation.

Moreover, the type of circulation pattern plays a role: atmospheric advection is accomplished by e.g. large-scale planetary waves—also known as Rossby waves, synoptic-scale waves such as cyclones, and other smaller perturbations for instance at the mesoscale. The atmospheric waves impact Arctic weather and climate (Rydsaa et al. 2021), and the planetary waves have a much larger potential to cause warming over the Arctic than the smaller waves including cyclones, since the Rossby waves in comparison with cyclones can affect a much larger area by simultaneous energy convergence (Graversen and Burtu 2016). Hence in the following the atmospheric energy transport is decomposed into a dry-static and a latent part and further into contributions from Rossby waves and synoptic waves, where the latter are associated with cyclones and mesoscale waves and other small-scale disturbances. This decomposition provides four energy transport components, a dry-static planetary, latent planetary, dry-static synoptic, and a latent synoptic component. In order to reveal the physical and statistical linkage between transport components and the SMB, regressions of the SMB on the transport components are investigated.

In general, the large-scale waves cause melting over Greenland for the dry-static part whereas the latent component leads to an overall positive mass balance (Fig. 2a, c). The increase in the SMB caused by the planetary latent component indicates that advection of moisture over Greenland is associated with an increase in precipitation, and that this precipitation effect is exceeding the melting associated with increased energy transfer to the surface. Note that the latent energy convergence leads to increase in energy transfer to the surface due to atmospheric warming by condensation, but more importantly due to an increase in atmospheric humidity and clouds enhancing surface downwelling longwave radiation. In addition a melting effect is induced by cooling rain water in the snowpack (see Sect. 2.2).

The synoptic waves, in fact, lead to a positive mass balance for the dry-static part, and for the latent component a pattern of negative mass balance at the margins of the ice-sheet and positive mass balance in the interior (Fig. 2b, d). At a first glance, these results may appear counter-intuitive. However, the regressions are affected by correlation between the transport components: for instance cyclones simultaneously bring heat and moisture into Greenland and hence contribute to both the dry-static and latent synoptic transport component (see Appendix). If decorrelation with the other transport components is applied, both dry-static components cause melting over Greenland, whereas those of the latent type lead to a positive mass balance (Fig. S3a–d). Hence, both planetary and synoptic waves play a considerable role
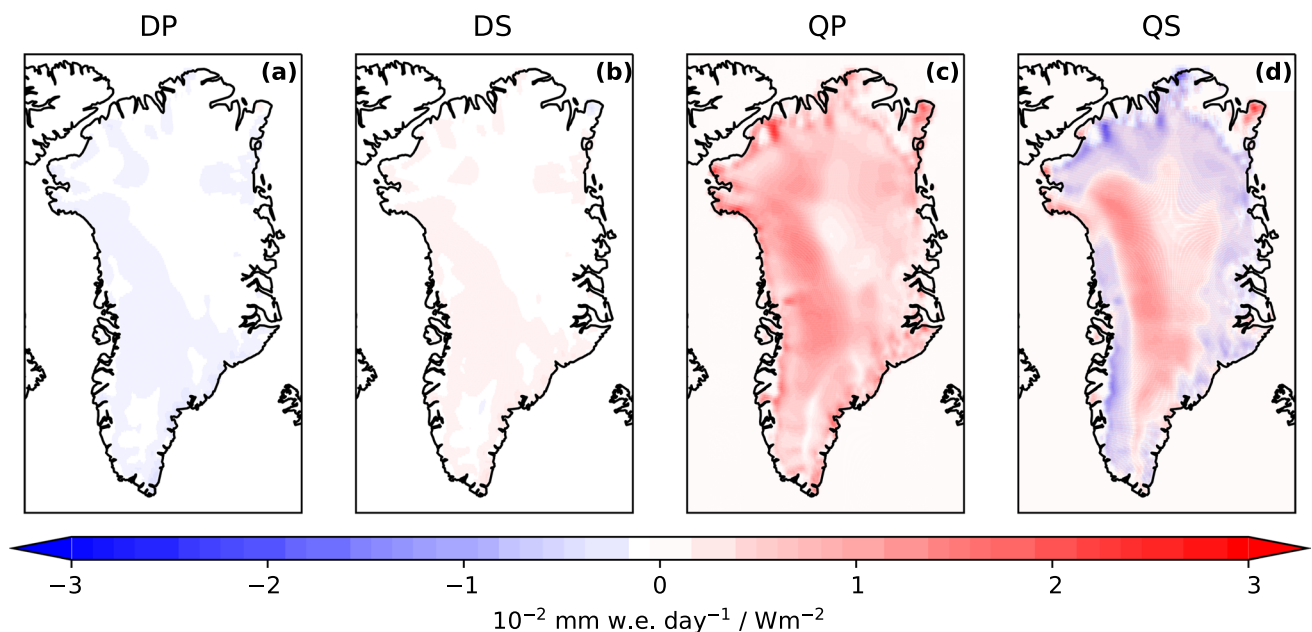

Fig. 2 Impact of the energy-transport components on the SMB. Regression of SMB on convergence of the planetary-scale dry-static transport (**a**), synoptic-scale dry-static transport (**b**), planetary-scale latent-heat transport (**c**), and synoptic-scale latent-heat transport (**d**). Virtually all shaded areas are significant on the 99% level based on a Monte-Carlo approach randomly interchanging phases (Fig. S2). The corresponding decorrelated parts, where each transport component is decorrelated with the three other components (see Appendix), are shown in Fig. S3a–d

for both melting and precipitation over the ice sheet, consistent with earlier findings (Oltmanns et al. 2019).

A decomposition into seasons shows that regressions associated with the dry-static transport convergence are the strongest in the summer season and weakest in the winter season (Fig. S4a, b, e, f), in particular the decorrelated parts show that both the planetary and synoptic types lead to stronger melting in summer than in winter (Fig. S3a, b, i, j). For the latent part, regressions are stronger in the winter season (Fig. S4c, d, g, h), but as indicated by the decorrelated parts, in both seasons both wave types cause about equal SMB impact (Fig. S3g, h, k, l). Although magnitudes of the regressions are in general different between seasons,

the patterns are the same and we therefore continue with a yearly perspective in the following analyses.

3.3 Trend in surface mass balance

The Greenland ice sheet SMB was close to a net zero balance—at least from the 1960s to 1990s (Graversen et al. 2011; Mouginot et al. 2019; IMBIETeam 2020), after which a negative trend has emerged (Figs. 3b, c and S6). Hence, the melt of the Greenland ice sheet shows a non-linear evolution relative to the ongoing, gradually increasing global warming. Given the strong impact of atmospheric circulation on the Greenland SMB, such a non-linear coupling between the
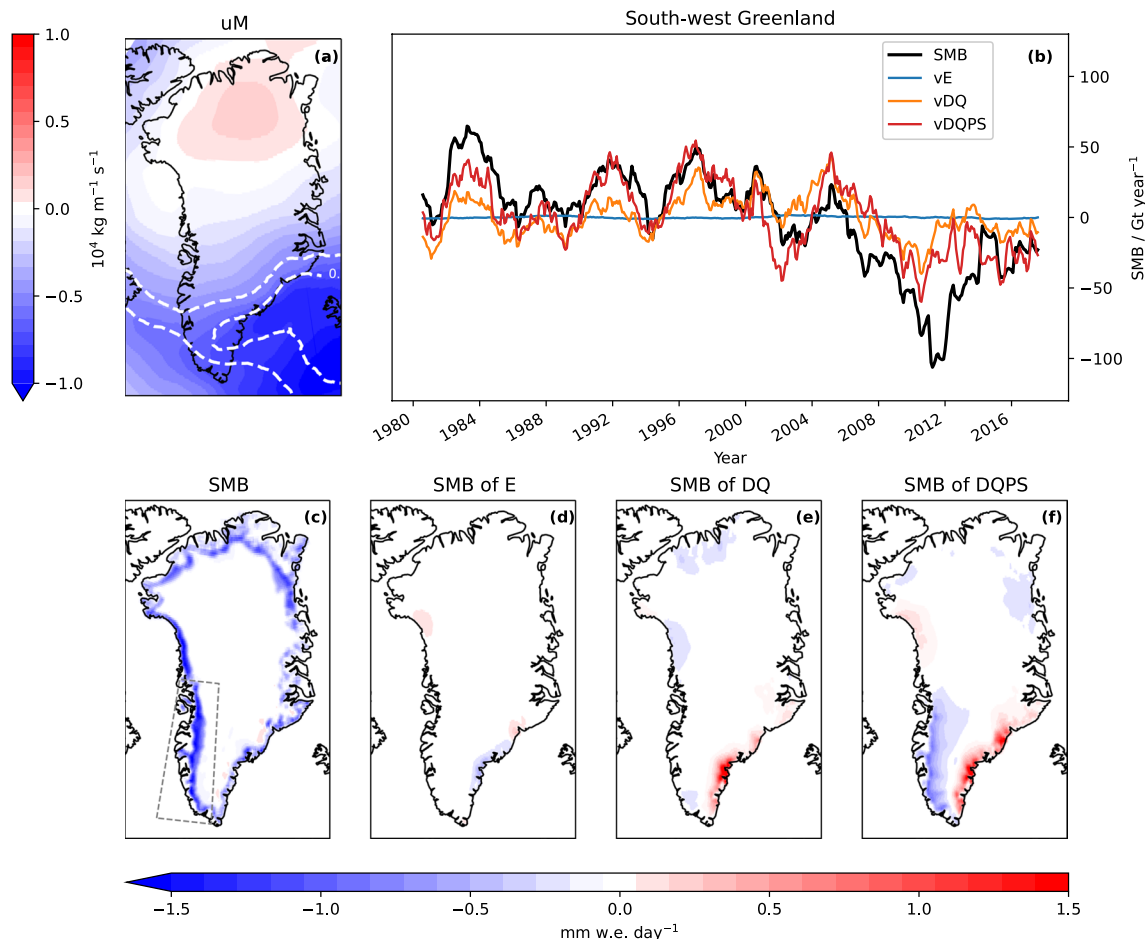

Fig. 3 Trend of the zonal mass flux and the surface mass balance and its components associated with the energy transport. Trends are difference in means over the years 2000–2018 and 1979–1999 and are shown for the zonal mass flux (**a**), the SMB (**c**), the part of the SMB associated with the total energy transport (**d**), the sum of the parts associated with the dry-static and latent transport separately (**e**), and the sum of the parts associated with the four individual components separately: planetary-scale and synoptic-scale dry-static and latent-heat transports (**f**). Time development of SMB-related fields averaged over southwest Greenland (area between 60° and 50° W and 60° and 72° N, indicated by the dashed, gray box in panel **c**, is shown in

panel **b** for the SMB (black), the part of the SMB associated with the total energy transport (blue), the sum of the parts of the SMB associated with the dry-static and latent transport (orange), and the sum of the parts of the SMB associated with the four individual transport components (red). A 36-month running average is applied to the time series in panel **b**. White, dashed lines in panel **a** indicate significance on a 90 and 95% level based on a Monte-Carlo approach randomly inter-changing years. Virtually all shaded areas in panels **d**–**f** are significant on the 99% level based on a Monte-Carlo approach randomly interchanging phases (Fig. S5)

ongoing climate change and the Greenland ice-sheet melt can emerge if the atmospheric circulation responds irregularly and intermittently abruptly to global warming. Indication that atmospheric circulation plays an important role for decadal variability of the Greenland SMB is provided by a change in the zonal (eastward) atmospheric mass flux over Greenland (Figs. 3a and S7). In the southern part of Greenland, the mass flux shows a clear and significant decrease between decades after and before year 2000. The mass flux brings energy and water vapour to Greenland, and a change of the mass flux will therefore affect the Greenland SMB. Accordingly, the zonal Rossby wave transport of both dry-static and latent heat has likewise decreased in the southern part of Greenland (Fig. 4a, c).

The difference of Greenland SMB between the period of trend (2000–2018) and the period of stability (1979–1999) shows that in recent decades, melt has been the strongest in the southwestern part of Greenland (Hanna et al. 2002; Mouginot et al. 2019; Fig. 3b, c), hence in the region of atmospheric mass-flux decrease (Figs. 3a and S6). In general, a negative SMB trend is encountered along the margins of the ice sheet except in parts of the mountainous areas in the southeastern part (Fig. 3c).

3.4 Circulation changes causing ice melt

A change in Rossby waves has in general increased convergence of dry-static energy transport over Greenland, although a decrease is found mainly in the mountains in the southeast and at the central-western ice-sheet margin (Fig. 5a). An opposite pattern has emerged for dry-static synoptic waves (Fig. 5b). However, if only the part of the

convergence that is decorrelated from the other components is considered, the two types of waves show a similar pattern with increased convergence over most part of Greenland but a decrease in the mountains in the southeast (Fig. S8a, b). In particular, both components show the strongest increase over northwest Greenland at latitudes where the zonal atmospheric mass flux is marginally changed (Fig. 3a), indicating that for an unchanged background mass flow, the waves bring more heat from the west into Greenland due to a general atmospheric warming. In the southwestern part, a reduction of the zonal mass flow compensates the effect of the overall atmospheric heating resulting in a more moderate and insignificant increase in energy convergence for the Rossby wave part, and even a small decrease in convergence for the part associated with synoptic waves (Fig. S8a, b).

A combination of regressions and trends (see Sect. 2.3) indicates that in southwestern Greenland the change in both the Rossby-wave and synoptic-wave transport of dry-static energy—although of opposite sign—have induced melting (Fig. 6a, b). Hence, an increase in energy convergence by Rossby waves in this region has led to melting, but perhaps counter-intuitively, a decrease in convergence by synoptic waves also has caused melting. The latter is due to the dominance of the effect of precipitation for the correlated part of the synoptic type inducing a positive SMB (Fig. 2b), and implying that a negative trend in transport convergence leads to a negative trend in SMB.

A change in Rossby waves has brought less water vapour into the southwestern part, but more to the mountains in the southeast, whereas roughly the opposite pattern is the case for the synoptic waves (Fig. 5c, d), although these patterns partly are associated with correlation with the other transport
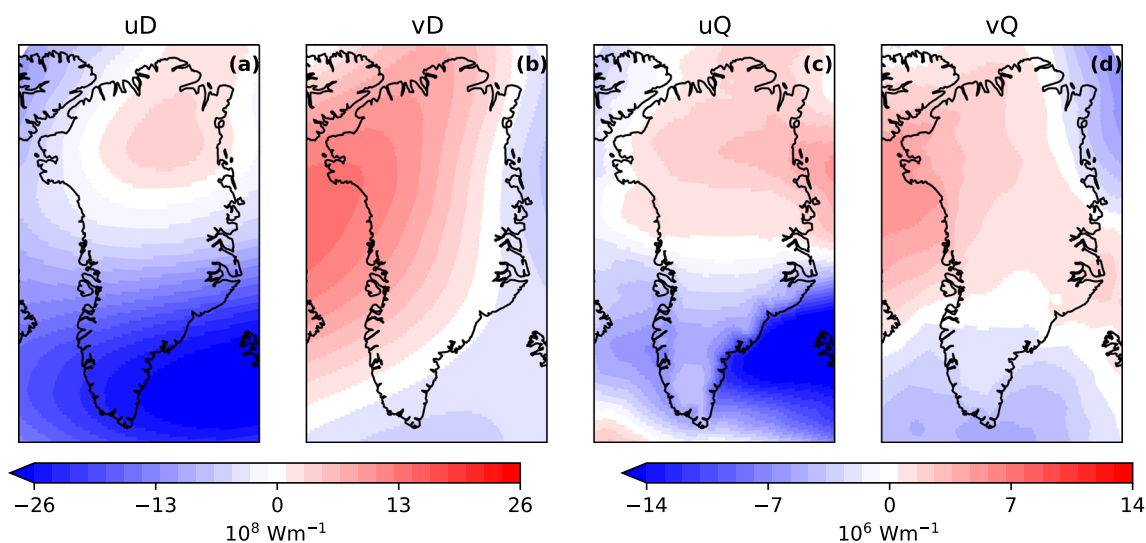

Fig. 4 As Fig. 3a but for Rossby wave zonal dry-static energy transport (**a**), meridional dry-static energy transport (**b**), zonal latent-heat transport (**c**), and meridional latent-heat transport (**d**)
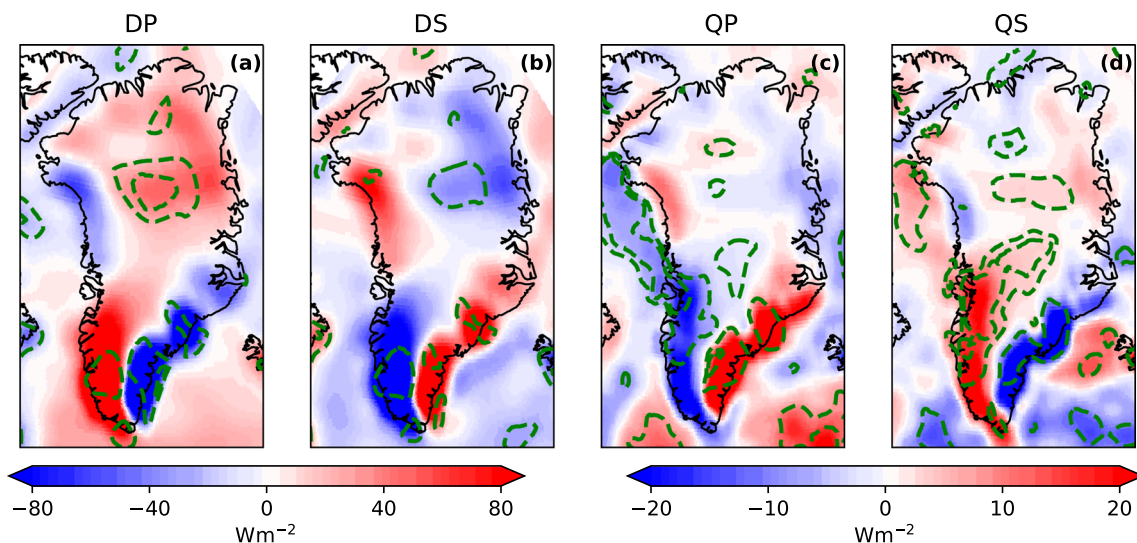
Fig. 5 As Fig. 2 but for trends of energy transport convergence of the four transport components. The trends are computed as the difference in mean over the years 2000–2018 and 1979–1999. The green, dashed lines denote the statistical significance of the trends on a 90 and 95% level based on a Monte-Carlo approach randomly inter-changing years (see Sect. 2.4). The corresponding decorrelated parts, where each transport component is decorrelated with the three other components (see Appendix), are shown in Fig. S8
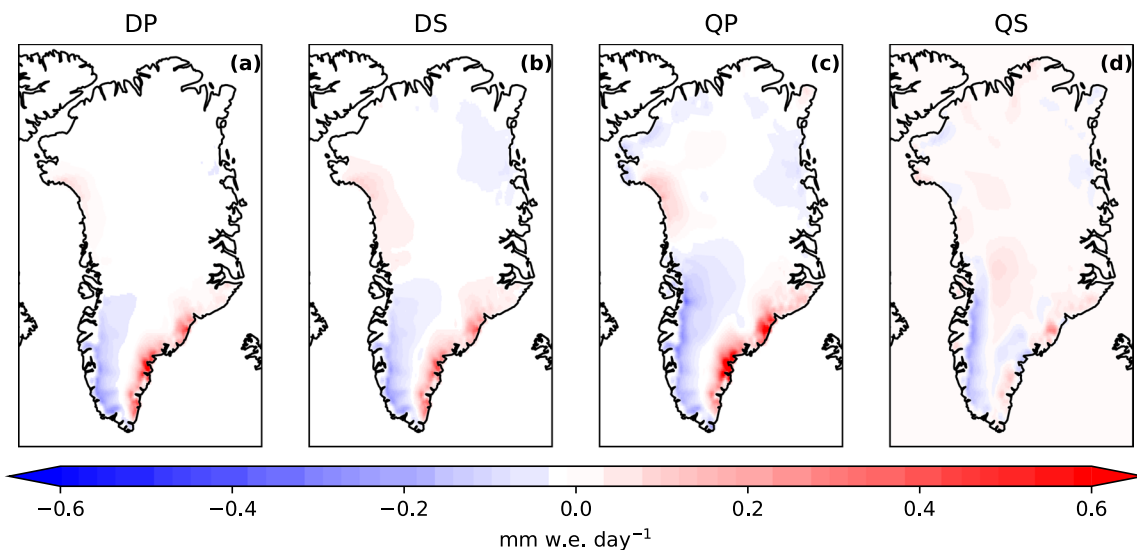
Fig. 6 As Fig. 2 but for SMB trends associated with trends in the transport convergence of the four energy-transport components, calculated by multiplying regression coefficients (Fig. 2) and trends (Fig. 5; see Sect. 2.4). Virtually all shaded areas in **d**–**f** are significant on the 99% level based on a Monte-Carlo approach randomly inter-changing phases (Fig. S9). The corresponding decorrelation analysis, where each transport component is decorrelated with the three other components (see Appendix), are shown in Fig. S10

components since the decorrelated parts show much smaller changes (Fig. S8c, d). Hence in the southwestern part the latent transport has shifted from the larger to the smaller wave types. This shift is consistent with the reduction in the atmospheric eastward mass flux in this region, reducing the moisture advection by the large-scale waves (Figs. 3a and 4c), and possibly also with a trend towards more open water in the Labrador Sea favouring an increase in cyclogenesis and latent heat release. Since the convergence of latent transport by the synoptic waves is associated with melting, and the opposite is the case the Rossby wave transport (Fig. 2c, d), a shift of the latent transport from Rossby waves to synoptic waves has resulted in negative trends in SMB associated with both wave types (Figs. 6c, d). Therefore in sum, over the southwest Greenland, a change of both Rossby and synoptic waves have led to ice loss, both due to enhanced

melting from increase in convergence of heat by the dry-static components, and due to less accumulation associated with reduced convergence of water vapour.

For the change in Rossby-wave energy-transport convergence, an opposite pattern between the dry-static and latent components is found in the southern part of Greenland (Fig. 5a, c). The time-mean atmospheric zonal mass flow over Greenland is from west to east. The dry-static part shows a convergence increase at the upstream western side and a decrease at the downstream eastern side, and the opposite is the case for the latent transport (Fig. 5a, c). This is consistent with a decrease of the westerly, time-mean mass flow (Fig. 3a): Weakening westerly flow causes reduced transport of water vapour into the western part inducing a decrease in orographic precipitation here, and allows for an increased frequency of eastward transport events into the mountains at the eastern side increasing precipitation there. In addition, also associated with a weakening zonal flow, air masses have more time to diabatically cool when advected over the western part and thus are colder when arriving at the eastern part of southern Greenland, which induces increase in heating at the western part and cooling over the mountains in the east. This is supported by changes in the energy transport components of the Rossby waves (Fig. 4): The zonal dry-static component shows a decrease with a negative gradient eastward which is the largest in the southwest of Greenland (Fig. 4a). The zonal latent component is showing a similar pattern, but revealing the largest negative gradient in the southeast (Fig. 4c). These patterns are associated with heat convergence which is the largest in the southwest for the dry-static part, and in the southeast for the latent. The changes in convergence are partly compensated by the meridional components that show generally divergence in southern Greenland (since these components indicate increase in northward heatflow with latitude; Fig. 4b, d). For the dry-static component, the divergence of the zonal component is dominating in the southwest, whereas in the southeast the zonal component shows smaller gradients, and hence the convergence by the meridional component dominates the change. The decrease in the time-mean zonal flow is consistent with the hypothesis concerning a general tendency of weather systems to become more stationary (Francis and Vavrus 2012; Kornhuber and Tamarin-Brodsky 2021), a hypothesis that is still under debate.

Regarding the effect of Rossby waves versus that of synoptic waves, the latter have been equally or more important when considering the SMB shift around year 2000 (Fig. 6). The important role of the small-scale waves in the recent evolution of the SMB, is consistent with projected changes of an increase in cyclones propagating over Greenland (Schuenemann and Cassano 2010).

The sum of the contributions to the Greenland SMB change from the four transport components shows a similar pattern as the total SMB change in the southwestern part of Greenland, whereas in other parts differences prevail (Fig. 3c, f). Time series of the SMB and the part of the SMB controlled by the four components of the energy transport show strong correspondence, in particular in the southwestern region (Fig. 3b). The correspondence is found on both the yearly scale, but also with regard to trends indicating the important role of the atmospheric circulation in the sudden shift towards a negative SMB around year 2000. For the entire ice sheet, this correspondence still appears on the yearly scale, but the transport-induced SMB shows little overall change (Fig. S6), which is due to the increase in SMB induced by the atmospheric circulation in the mountains in the southeast. Hence, according to ERA5, at the ice-sheet margin in the mountainous southeastern part of Greenland, the circulation has induced an overall positive SMB, whereas little total SMB change is found by the RACMO model. The ERA5 results presented here only include the part of the SMB change linked to the circulation changes. Hence the discrepancy between the two data sets could reflect that positive SMB caused by the circulation changes is compensated by local melting or precipitation processes unrelated to the circulation. For example, this region is in the vicinity of a sea where sea ice seldomly forms, and local sea-surface temperature changes could alter local latent and sensible heat release affecting local clouds, precipitation, and surface energy balance.

The split of the energy transport by the atmospheric circulation into wave parts is important since these parts affect the SMB and its trend in different ways. If no separation into Rossby and synoptic waves is performed, but only a decomposition into dry-static and latent part, the circulation impact on the SMB trend in southwestern Greenland is less apparent (Fig. 3b, e), and if also the decomposition into dry-static and latent parts is disregarded, the SMB-trend signal essentially disappears (Fig. 3b, d).

4 Conclusions

Regression of the Greenland SMB on the components of the atmospheric energy transport, as we propose here, provides a more direct linkage between atmospheric circulation and the Greenland ice sheet melt than has previously been given. On yearly and interannual scales, the atmospheric circulation exerts a strong control on the SMB. Consequently, after year 2000, a change in atmospheric heat and moisture transport over Greenland has significantly affected the Greenland ice-sheet melt. In the southwestern part, where the ice melt is considerable, the eastward atmospheric mass flux over Greenland, and the part of the SMB that is linearly linked to circulation changes, both show a similar development as the total SMB. Based

on a decomposition of the circulation into components, it is evident that in this region the atmospheric circulation explains a considerable part of the ice-sheet melt. In the mountainous southeastern part of Greenland, the atmospheric circulation has induced a positive SMB change which, however, has had marginal effect on the total SMB, presumable due to compensation by melting and precipitation changes unrelated to the circulation, which needs further investigation.

It is likely that these circulation changes are coupled to global warming (Francis and Vavrus 2012; Kornhuber and Tamarin-Brodsky 2021), although this is still under debate (Barnes and Screen 2015; Cohen et al. 2018; Huguenin et al. 2020). A decrease in eastward mass flow over southern Greenland is consistent with a general reduction of the Northern-Hemisphere meridional temperature gradient, weakening the thermal wind and hence the mid-latitude westerlies. The reduction of the meridional temperature gradient is a well-established climate-change signal of Arctic temperature amplification—the Arctic warming pace being larger than that of the rest of the hemisphere. It has been argued that the atmospheric circulation change will amplify extreme weather events and hereby enhance severity of climate change (Francis and Vavrus 2012; Kornhuber and Tamarin-Brodsky 2021; White et al. 2022). The results presented here, regarding circulation impact on the Greenland ice-sheet melt, provide an additional example that atmospheric circulation change can have large regional and global consequences; in this case, as it leads to global sea-level rise.

Appendix: Decorrelation

Surface energy balance and precipitation both have strong but opposite impact on the Greenland SMB (Fig. 1). However, the two fields are often correlated since for instance humid air can lead to both positive surface energy balance and precipitation anomalies. The effect of precipitation on SMB associated with the surface energy balance can be suppressed by first performing a decorrelation of the surface energy balance with the precipitation before the SMB regression is computed. The decorrelated part of the surface energy balance is obtained as:

$$\text{SEB}_\perp(\phi, \lambda, t) = \text{SEB} - \beta_{\text{Pr}}^{\text{SEB}} \text{Pr}, \tag{11}$$

where $\text{SEB}(\phi, \lambda, t)$ and $\text{Pr}(\phi, \lambda, t)$ is the surface energy balance and precipitation field, respectively, and

$$\beta_{\text{Pr}}^{\text{SEB}} = \frac{\text{cov}[\text{SEB}, \text{Pr}]}{\text{var}[\text{Pr}]} \tag{12}$$

is the regression of SEB on Pr. Now, by construction:

$$\beta_{\text{Pr}}^{\text{SEB}_\perp} = \frac{\text{cov}\left[\text{SEB}_\perp, \text{Pr}\right]}{\text{var}[\text{Pr}]} = 0, \tag{13}$$

and $\text{SEB}_\perp$ and Pr are orthogonal. Hence Fig. 1b shows regression of SMB on $\text{SEB}_\perp$.

Likewise the four considered components of the energy transport (planetary and synoptic components of both dry-static and latent parts) are temporal correlated with each other. For example, a large-scale Rossby wave reaching land will partly become dissolved into smaller-scale structures due to the impact of the orography. Therefore the small-scale waves are to some extent dependent on—and hence correlated with—those at the larger scales. In addition waves may simultaneously bring both sensible heat and water vapour inducing a temporal correlation between dry-static and latent transport components. Since the four components affect the SMB differently, and in order to investigate the physical processes associated with the convergence of the individual components, each component is split into a decorrelated and a correlated part. The decorrelated parts are constructed as:

$$
\begin{aligned}
D_{p\perp}^{\text{conv}}(\phi, \lambda, t) &= \langle\langle\langle D_p^{\text{conv}} | D_s^{\text{conv}}\rangle | Q_p^{\text{conv}}\rangle | Q_s^{\text{conv}}\rangle, \\
D_{s\perp}^{\text{conv}}(\phi, \lambda, t) &= \langle\langle\langle D_s^{\text{conv}} | D_p^{\text{conv}}\rangle | Q_p^{\text{conv}}\rangle | Q_s^{\text{conv}}\rangle, \\
Q_{p\perp}^{\text{conv}}(\phi, \lambda, t) &= \langle\langle\langle Q_p^{\text{conv}} | Q_s^{\text{conv}}\rangle | D_p^{\text{conv}}\rangle | D_s^{\text{conv}}\rangle, \\
Q_{s\perp}^{\text{conv}}(\phi, \lambda, t) &= \langle\langle\langle Q_s^{\text{conv}} | Q_p^{\text{conv}}\rangle | D_p^{\text{conv}}\rangle | D_s^{\text{conv}}\rangle,
\end{aligned} \tag{14}
$$

where

$$\langle A|B\rangle = A - \beta_B^A \times B \quad \text{and} \quad \beta_B^A = \frac{\text{cov}[A, B]}{\text{var}[B]}. \tag{15}$$

The correlated part of the energy convergence of dry-static planetary waves is given as:

$$D_{p\|}^{\text{conv}} = D_p^{\text{conv}} - D_{p\perp}^{\text{conv}}, \tag{16}$$

and similarly for the other transport components. Note that although $A_\perp = \langle A|B\rangle$ is orthogonal to B, similar to the case in Eq. 13, the $\langle \cdot | \cdot \rangle$ operation is nonlinear. Hence it does not hold that the decorrelated part of the dry-static planetary energy convergence is orthogonal to the three other components, although the correlations with these components are reduced.

Figures S3 and S8 show regression of the SMB on the energy transport based on the decorrelated part of the transport components, and Fig. S10 shows SMB trends explained by the energy transport based on the sum of the contribution from the decorrelated and correlated parts of each transport component.

Declarations

References

Baggett C, Lee S (2015) Arctic warming induced by tropically forced tapping of available potential energy and the role of the planetary-scale waves. J Atmos Sci 72(4):1562–1568

Barnes EA, Screen JA (2015) The impact of arctic warming on the midlatitude jet-stream: can it? has it? will it? Wiley Interdiscip Rev: Clim Change 6(3):277–286

Barrett BS, Henderson GR, McDonnell E et al (2020) Extreme Greenland blocking and high-latitude moisture transport. Atmos Sci Lett 21(11):e1002

Bevis M, Harig C, Khan SA et al (2019) Accelerating changes in ice mass within Greenland, and the ice sheet's sensitivity to atmospheric forcing. Proc Natl Acad Sci 116(6):1934–1939

Choi Y, Morlighem M, Rignot E et al (2021) Ice dynamics will remain a primary driver of Greenland ice sheet mass loss over the next century. Commun Earth Environ 2(1):26

Cohen J, Pfeiffer K, Francis JA (2018) Warm arctic episodes linked with increased frequency of extreme winter weather in the United States. Nat Commun 9(1):869

Ding Q, Wallace JM, Battisti DS et al (2014) Tropical forcing of the recent rapid arctic warming in northeastern Canada and Greenland. Nature 509(7499):209–212

Doyle SH, Hubbard A, Van De Wal RS et al (2015) Amplified melt and flow of the Greenland ice sheet driven by late-summer cyclonic rainfall. Nat Geosci 8(8):647–653

Ettema J, Van den Broeke M, Van Meijgaard E et al (2010) Climate of the Greenland ice sheet using a high-resolution climate model—part 1: evaluation. Cryosphere 4(4):511–527

Fausto RS, van As D, Box JE et al (2016) The implication of non-radiative energy fluxes dominating Greenland ice sheet exceptional ablation area surface melt in 2012. Geophys Res Lett 43(6):2649–2658

Fettweis X, Hanna E, Lang C et al (2013) Brief communication "Important role of the mid-tropospheric atmospheric circulation in the recent surface melt increase over the Greenland ice sheet''. Cryosphere 7(1):241–248

Fettweis X, Hofer S, Krebs-Kanzow U et al (2020) GrSMBMIP: inter-comparison of the modelled 1980–2012 surface mass balance over the Greenland ice sheet. Cryosphere Discuss 2020:1–35

Francis JA, Vavrus SJ (2012) Evidence linking arctic amplification to extreme weather in mid-latitudes. Geophys Res Lett 39(6)

Graham RM, Cohen L, Ritzhaupt N et al (2019) Evaluation of six atmospheric reanalyses over Arctic sea ice from winter to early summer. J Clim 32(14):4121–4143

Graversen RG (2006) Do changes in the midlatitude circulation have any impact on the Arctic surface air temperature trend? J Clim 19(20):5422–5438

Graversen RG, Burtu M (2016) Arctic amplification enhanced by latent energy transport of atmospheric planetary waves. Q J R Meteorol Soc 142(698):2046–2054

Graversen RG, Mauritsen T, Drijfhout S et al (2011) Warm winds from the Pacific caused extensive Arctic sea-ice melt in summer 2007. Clim Dyn 36:2103–2112

Hanna E, Huybrechts P, Mote TL (2002) Surface mass balance of the Greenland ice sheet from climate-analysis data and accumulation/runoff models. Ann Glaciol 35:67–72

Hanna E, Navarro FJ, Pattyn F et al (2013) Ice-sheet mass balance and climate change. Nature 498(7452):51–59

Hanna E, Fettweis X, Mernild SH et al (2014) Atmospheric and oceanic climate forcing of the exceptional Greenland ice sheet surface melt in summer 2012. Int J Climatol 34(4):1022–1037

Hanna E, Cropper TE, Hall RJ et al (2016) Greenland Blocking Index 1851–2015: a regional climate change signal. Int J Climatol 36(15):4847–4861

Hanna E, Fettweis X, Hall RJ (2018) Brief communication: Recent changes in summer Greenland blocking captured by none of the CMIP5 models. Cryosphere 12(10):3287–3292

Hanna E, Pattyn F, Navarro F et al (2020) Mass balance of the ice sheets and glaciers—progress since AR5 and challenges. Earth Sci Rev 201:102976

Hanna E, Cappelen J, Fettweis X et al (2021) Greenland surface air temperature changes from 1981 to 2019 and implications for ice-sheet melt and mass-balance change. Int J Climatol 41:E1336–E1352

Heiskanen T, Graversen RG, Rydsaa JH et al (2020) Comparing wavelet and Fourier perspectives on the decomposition of meridional energy transport into synoptic and planetary components. Q J R Meteorol Soc 146(731):2717–2730

Henderson GR, Barrett BS, Wachowicz LJ et al (2021) Local and remote atmospheric circulation drivers of Arctic change: a review. Front Earth Sci 9:709896

Hersbach H, Bell B, Berrisford P et al (2020) The ERA5 global reanalysis. Q J R Meteorol Soc 146(730):1999–2049

Hofer S, Tedstone AJ, Fettweis X et al (2017) Decreasing cloud cover drives the recent mass loss on the Greenland ice sheet. Sci Adv 3(6):e1700584

Huguenin MF, Fischer EM, Kotlarski S et al (2020) Lack of change in the projected frequency and persistence of atmospheric circulation types over Central Europe. Geophys Res Lett 47(9):e2019GL086132

IMBIETeam (2020) Mass balance of the Greenland ice sheet from 1992 to 2018. Nature 579(7798):233–239

Inall ME, Murray T, Cottier FR et al (2014) Oceanic heat delivery via Kangerdlugssuaq Fjord to the south-east Greenland ice sheet. J Geophys Res: Oceans 119(2):631–645

IPCC (2021) Climate Change 2021: The Physical Science Basis. Contribution of Working Group I to the Sixth Assessment Report of the Intergovernmental Panel on Climate Change. In: Masson-Delmotte V, Zhai P, Pirani A, Connors SL, Péan C, Berger S, Caud N, Chen Y, Goldfarb L, Gomis MI, Huang M, Leitzell K, Lonnoy E, Matthews JBR, Maycock TK, Waterfield T, Yelekçi O, Yu R, Zhou B (eds) Cambridge University Press, Cambridge, United Kingdom and New York, NY, USA, pp. 2391. https://doi.org/10.1017/9781009157896

Izeboud M, Lhermitte S, Van Tricht K et al (2020) The spatiotemporal variability of cloud radiative effects on the Greenland ice sheet surface mass balance. Geophys Res Lett 47(12):e2020GL087315

Kapsch ML, Skific N, Graversen RG et al (2019) Summers with low Arctic sea ice linked to persistence of spring atmospheric circulation patterns. Clim Dyn 52:2497–2512

Katsman CA, Sterl A, Beersma J et al (2011) Exploring high-end scenarios for local sea level rise to develop flood protection strategies for a low-lying delta-the Netherlands as an example. Clim Change 109:617–645

King MD, Howat IM, Candela SG et al (2020) Dynamic ice loss from the Greenland ice sheet driven by sustained glacier retreat. Commun Earth Environ 1(1):1

Kornhuber K, Tamarin-Brodsky T (2021) Future changes in Northern Hemisphere summer weather persistence linked to projected Arctic warming. Geophys Res Lett 48(4):e2020GL091603

Lamarche-Gagnon G, Wadham JL, Sherwood Lollar B et al (2019) Greenland melt drives continuous export of methane from the ice-sheet bed. Nature 565(7737):73–77

Matsumura S, Yamazaki K, Suzuki K (2021) Slow-down in summer warming over Greenland in the past decade linked to central Pacific El Niño. Commun Earth Environ 2(1):257

Mattingly K, Mote T, Fettweis X (2018) Atmospheric river impacts on Greenland ice sheet surface mass balance. J Geophys Res: Atmos 123(16):8538–8560

Mattingly KS, Mote TL, Fettweis X et al (2020) Strong summer atmospheric rivers trigger Greenland ice sheet melt through spatially varying surface energy balance and cloud regimes. J Clim 33(16):6809–6832

Mote TL (1998) Mid-tropospheric circulation and surface melt on the Greenland ice sheet. Part I: atmospheric teleconnections. Int J Climatol: J R Meteorol Soc 18(2):111–129

Mouginot J, Rignot E, Bjørk AA et al (2019) Forty-six years of Greenland ice sheet mass balance from 1972 to 2018. Proc Natl Acad Sci 116(19):9239–9244

Niwano M, Box J, Wehrlé A et al (2021) Rainfall on the Greenland ice sheet: present-day climatology from a high-resolution non-hydrostatic polar regional climate model. Geophys Res Lett 48(15):e2021GL092942

Noël B, Van De Berg WJ, Van Wessem JM et al (2018) Modelling the climate and surface mass balance of polar ice sheets using RACMO2—part 1: Greenland (1958–2016). Cryosphere 12(3):811–831

Nygård T, Naakka T, Vihma T (2020) Horizontal moisture transport dominates the regional moistening patterns in the Arctic. J Clim 33(16):6793–6807

Oltmanns M, Straneo F, Tedesco M (2019) Increased Greenland melt triggered by large-scale, year-round cyclonic moisture intrusions. Cryosphere 13(3):815–825

Oort AH, Peixóto JP (1983) Global angular momentum and energy balance requirements from observations. In: Saltzman B (ed) Advances in geophysics, vol 25. Elsevier, Amsterdam, pp 355–490

Rydsaa JH, Graversen R, Heiskanen TIH et al (2021) Changes in atmospheric latent energy transport into the Arctic: planetary versus synoptic scales. Q J R Meteorol Soc 147(737):2281–2292

Schuenemann KC, Cassano JJ (2010) Changes in synoptic weather patterns and Greenland precipitation in the 20th and 21st centuries: 2. Analysis of 21st century atmospheric changes using self-organizing maps. J Geophys Res: Atmos 115(D5)

Sherman P, Tziperman E, Deser C et al (2020) Historical and future roles of internal atmospheric variability in modulating summertime Greenland ice sheet melt. Geophys Res Lett 47(6):e2019GL086913

Slater D, Straneo F (2022) Submarine melting of glaciers in Greenland amplified by atmospheric warming. Nat Geosci 15(10):794–799

Sundal AV, Shepherd A, Nienow P et al (2011) Melt-induced speed-up of Greenland ice sheet offset by efficient subglacial drainage. Nature 469(7331):521–524

Trenberth KE (1991) Climate diagnostics from global analyses: conservation of mass in ECMWF analyses. J Clim 4(7):707–722

van den Broeke M, Box J, Fettweis X et al (2017) Greenland ice sheet surface mass loss: recent developments in observation and modeling. Curr Clim Change Rep 3:345–356

van Kampenhout L, Lenaerts JT, Lipscomb WH et al (2020) Present-day Greenland ice sheet climate and surface mass balance in CESM2. J Geophys Res: Earth Surf 125(2):e2019JF005318

Wachowicz LJ, Preece JR, Mote TL et al (2021) Historical trends of seasonal Greenland blocking under different blocking metrics. Int J Climatol 41:E3263–E3278

White RH, Kornhuber K, Martius O et al (2022) From atmospheric waves to heatwaves: a waveguide perspective for understanding and predicting concurrent, persistent, and extreme extratropical weather. Bull Am Meteorol Soc 103(3):E923–E935

Wood M, Rignot E, Fenty I et al (2021) Ocean forcing drives glacier retreat in Greenland. Sci Adv 7(1):eaba7282

Yang H, Krebs-Kanzow U, Kleiner T et al (2022) Impact of paleoclimate on present and future evolution of the Greenland ice sheet. PLoS One 17(1):e0259816